MASSACHUSETTS INSTITUTE OF TECHNOLOGY

LINCOLN LABORATORY

MONOPULSE FAR-FIELD PATTERNS

Sheldon S. Sandler

Approved Leon J. Ricardi

Group Report No. 315-1

July 23, 1959

The work reported in this document was performed by Lincoln Laboratory, a center for research operated by Massachusetts Institute of Technology; this work was supported by the U. S. Air Force under Air Force Contract No. AF 19(604)-5200.

LEXINGTON MASSACHUSETTS

MONOPULSE FAR-FIELD PATTERNS

I. INTRODUCTION

A general theory of monopulse tracking radars will be found in a recent book by Rhodes[1]. The present paper will serve as an adjunct to the monopulse problem, i.e. the analytical prediction of far-field patterns. The theoretical prediction of monopulse radiation patterns should prove useful for antenna system comparison.

An idealized two-horn monopulse system is shown in Figure 1. Two primary sources are located symmetrically with respect to the focal axis. The sources are polarized in the x-direction and their back radiation is neglected. The two sources may be fed either in-phase or 180 degrees out-of-phase. The two fundamental sources of tracking information are the sum (in-phase) and difference (out-of-phase) radiation patterns. The quantities of interest are (1) the maximum gain of the sum pattern (2) the angular sensitivity of the difference pattern near boresight and (3) the product of (1) and (2) above.

The radiation pattern will be calculated by two different methods:

1. Current distribution method suitable for machine computation.
2. Scalar diffraction theory (analytical expressions).

The theoretical results will be presented for the case of rectangular waveguide illumination.

II. THEORY

The physical arrangement of the primary sources allows some simplification in the analytical formulation. Since the structure is symmetrical about the x-z plane (see Figure 1), then it is only necessary to consider the secondary radiation pattern due to a source placed at $y = m$. The field for a similar source placed at $y = m$ is obtained directly by replacing m by -m.

The problem of determining the radiation pattern for a single offset source has been solved by this author in a previous paper[2]. Confining attention to the H-plane, then the radiation field for a source placed at y = m is given by Equation A-14 and A-15 in integral form (the letter A refers to Reference 2). Symbolically the radiation field is given by

$$\bar{E}_H(\theta, \tfrac{\pi}{2}; m) = E_\theta(\theta, \tfrac{\pi}{2}; m)\hat{i}_\theta + E_\phi(\theta, \tfrac{\pi}{2}; m)\hat{i}_\phi \qquad (1)$$

where $\hat{i}_\theta$ and $\hat{i}_\phi$ are the unit far-field vectors shown in Figure 1. The field pattern for the case of two sources fed in phase becomes

$$\bar{E}_{HS}(\theta, \tfrac{\pi}{2}) = \bar{E}_H(\theta, \tfrac{\pi}{2}; m) + \bar{E}_H(\theta, \tfrac{\pi}{2}; -m) \qquad (2)$$

Similarly the field pattern for the case of out-of-phase primary illumination is given by

$$\bar{E}_{HD}(\theta, \tfrac{\pi}{2}) = \bar{E}_H(\theta, \tfrac{\pi}{2}; m) - \bar{E}_H(\theta, \tfrac{\pi}{2}; -m) \qquad (3)$$

Note that the rigorous current distribution formulation includes the effect of the cross-polarization component of the radiation field. The scalar diffraction solution considers only the main polarization component, i.e. the x-component. The sum and difference patterns may be calculated from Equations 2, 3, A-37 and A-67, whence

$$E_{HS} \doteq \Lambda_1(\beta) - M_{11}\Lambda_2(\beta) - [M_{21} + M_{31}\sin\theta]\Lambda_3(\beta) \qquad (4)$$

where

$$M_{11} = \frac{k^2a^2}{16f^2}\left\{1 - 4\left(\frac{a}{2f}\right)^2\left[1 - \left(\frac{a}{2f}\right)^2\right]\right\}\left[\left(m + \frac{b}{2}\right)^2 + \left(m - \frac{b}{2}\right)^2\right]$$

$$M_{21} = \frac{k^2a^2}{12f^2}\left(\frac{a}{2f}\right)^2\left[1 - 2\left(\frac{a}{2f}\right)^2\right]\left[\left(m + \frac{b}{2}\right)^2 + \left(m - \frac{b}{2}\right)^2\right]$$

$$M_{31} = \frac{k^2 a^2}{12 f}\left(\frac{a}{2f}\right)^2$$

$$\beta = ka \sin\theta \qquad\qquad \Lambda_p(\beta) = \frac{p!}{(\frac{\beta}{2})^p} J_p(\beta)$$

$$k = 2\pi/\lambda$$

a = aperture radius

and similarly for the difference pattern

$$E_{HD} = [M_{12} + M_{22}\sin\theta]\Lambda_2(\beta) + [M_{32} + M_{42}\sin\theta]\Lambda_3(\beta) \qquad (5)$$

where

$$M_{12} = \frac{3m}{2}\left(\frac{b}{\pi}\right)^2 \frac{k^2 a^2}{f^2}\left\{1 - 4\left(\frac{a}{2f}\right)^2\left[1 - \left(\frac{a}{2f}\right)^2\right]\right\}$$

$$M_{22} = \frac{k^2 a^2 m}{f}$$

$$M_{32} = \frac{k^2 a^2 m}{f^2}\left(\frac{a}{2f}\right)^2\left[1 - \left(\frac{a}{2f}\right)^2\right]\left(\frac{b}{\pi}\right)^2 + \frac{1}{12}\frac{\beta^2}{f}\left(\frac{a}{2f}\right)^4 k^2 \times \left[\left(m + \frac{b}{2}\right)^3 + \left(m - \frac{b}{2}\right)^3 - 6m\left(\frac{b}{\pi}\right)^2\right]$$

$$M_{42} = \frac{\beta^2}{24}\left(\frac{k^2 a^2}{2f^2}\right)\left[\left(m + \frac{b}{2}\right)^3 + \left(m - \frac{b}{2}\right)^3 - 6m\left(\frac{b}{\pi}\right)^2\right]$$

The limitations and assumptions inherent in the current distribution and diffraction formulations are given in Reference 2.

III. EXPERIMENTAL MEASUREMENTS

The experimental model is shown pictorially in Figure 2, and diagrammatically in Figure 3. The feed consists of two x-band waveguide sections which are mechanically connected by a high-pitch turnbuckle. Flexible sections connect the sources to the driving point located on the reverse side of the parabolic reflector. With the aid of the flexible sections, the motion of the feed waveguide was constrained to be parallel to the focal axis.

Since small variations in feed line length cause a large error in the relative driving phase, a precision phase shifter was employed. The mechanical alignment of the monopulse model was as follows:

1. The monopulse reflector and transmitter were optically boresighted.
2. The output of the two feed horns was directly connected to a magic tee. A detector was placed in the sum arm of the magic tee and connected to the input of a bolometer amplifier. The transmitter and monopulse reflector were mechanically adjusted to produce a maximum sum output.
3. Precision phase shifters were added between the feed horns and the magic tee. The detector was placed in the difference arm. The phase shifter was adjusted for a null on boresight. Mechanical alignment was rechecked.

The H-plane radiation patterns for in-phase and out-of-phase primary illumination were transcribed in a pattern recorder as a function of the far-field angle (H). The two quantities of interest, the sum gain at boresight and the angular sensitivity were determined graphically from the sum and difference recorder patterns.

III. THEORETICAL AND EXPERIMENTAL RESULTS

The theoretical results were calculated for the following antenna system:

Paraboloidal Reflector

f/D = 0.573 f = 27.5 inches

Primary Sources

X-band waveguide (.40 x .900 inches I.D.)

Frequency

9448 Mc.

As a basis of comparison, the feed tilt will be defined in terms of a standard beamwidth (SBW). A SBW is the half-power beamwidth of an equivalent paraboloid illuminated by a single dipole located at the focus. For the above system

one SBW equals 1.55 degrees. The radiation pattern for in-phase (sum) illumination is shown in Graphs 1, 2, 3 and 4. When the two feed guides are close (e.g. when the offset is equal to or less than .42 SBW) the main lobe has the same general shape as a single source pattern, but with an increased beamwidth. When the feed tilt is increased, the main lobe degenerates into two distinct maxima. Note that the theoretical patterns have been normalized relative to their maximum value, and the variation of gain with feed tilt must be taken into account when calculating relative side lobe levels, etc. The results for the analytical solution shown in Graph 3 indicates a higher side-lobe level than the current distribution method. The experimental results shown in Graph 4 are bracketed by the current distribution and scalar diffraction methods.

The variation of boresight gain with feed tilt is shown in Graph 5. The sum gain remains relatively constant up to a feed tilt of one-third beamwidth and then drops 10 db at one SBW feed tilt. The analytical formulation agrees well with the rigorous calculations. The experimental gain also lies between the results obtained by the two methods of calculation.

The difference patterns are shown in Graphs 6, 7, 8 and 9. For small values of feed tilt, the pattern shape remains somewhat fixed. At larger values of feed tilt the two symmetrical boresight lobes increase in width. The gain of the difference pattern remained constant over a range of feed tilts from 0.32 SBW to 1.11 SBW. This result is shown experimentally in Graph 9.

The sensitivity, or slope at boresight crossover, was calculated theoretically from the difference patterns. The theoretical and experimental sensitivities are compared in Graph 10.

The current distribution method indicates a linear increase in sensitivity with a maximum value near a feed tilt value of 0.6 SBW. Scalar diffraction theory predicts a monotonically increasing sensitivity for values of feed tilt less than 1.1 SBW. The experimental results exhibit a maximum value of sensitivity as per the current distribution calculations; however, the maximum value occurs at about one

SBW beam tilt. In monopulse systems the product of gain and sensitivity is of prime importance. This product is shown in Graph 11. The maximum value of the product occurs near a feed tilt of 0.42 SBW. As far as actual monopulse system operation is concerned, it should be noted (i.e. see Graph 5) that the sum gain decreases rapidly with increasing feed tilt. Hence, it would be advisable to choose the smallest feed tilt consistent with sensitivity requirements.

BIBLIOGRAPHY

1) Rhodes, Donald R., Introduction to Monopulse, McGraw-Hill, New York New York, 1959.

2) Sandler, Sheldon S., Paraboloidal Reflector Patterns for Off-Axis Feed, Lincoln Laboratory Technical Report #205.

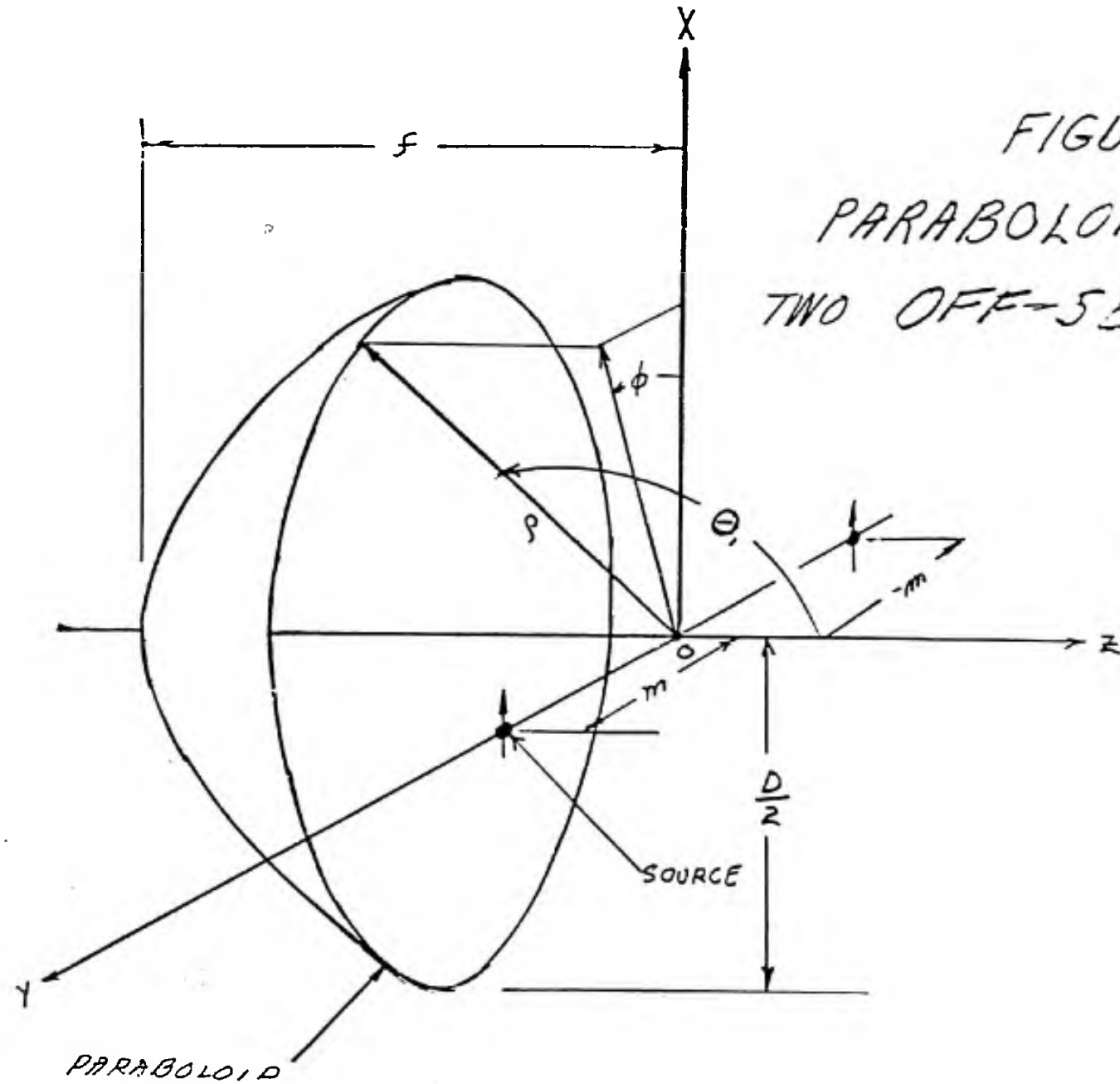

FIGURE I
PARABOLOID WITH
TWO OFF-SET FEEDS

$P(R, \Theta, \Phi)$

H-PLANE ~ $\Phi = \frac{\pi}{2}$

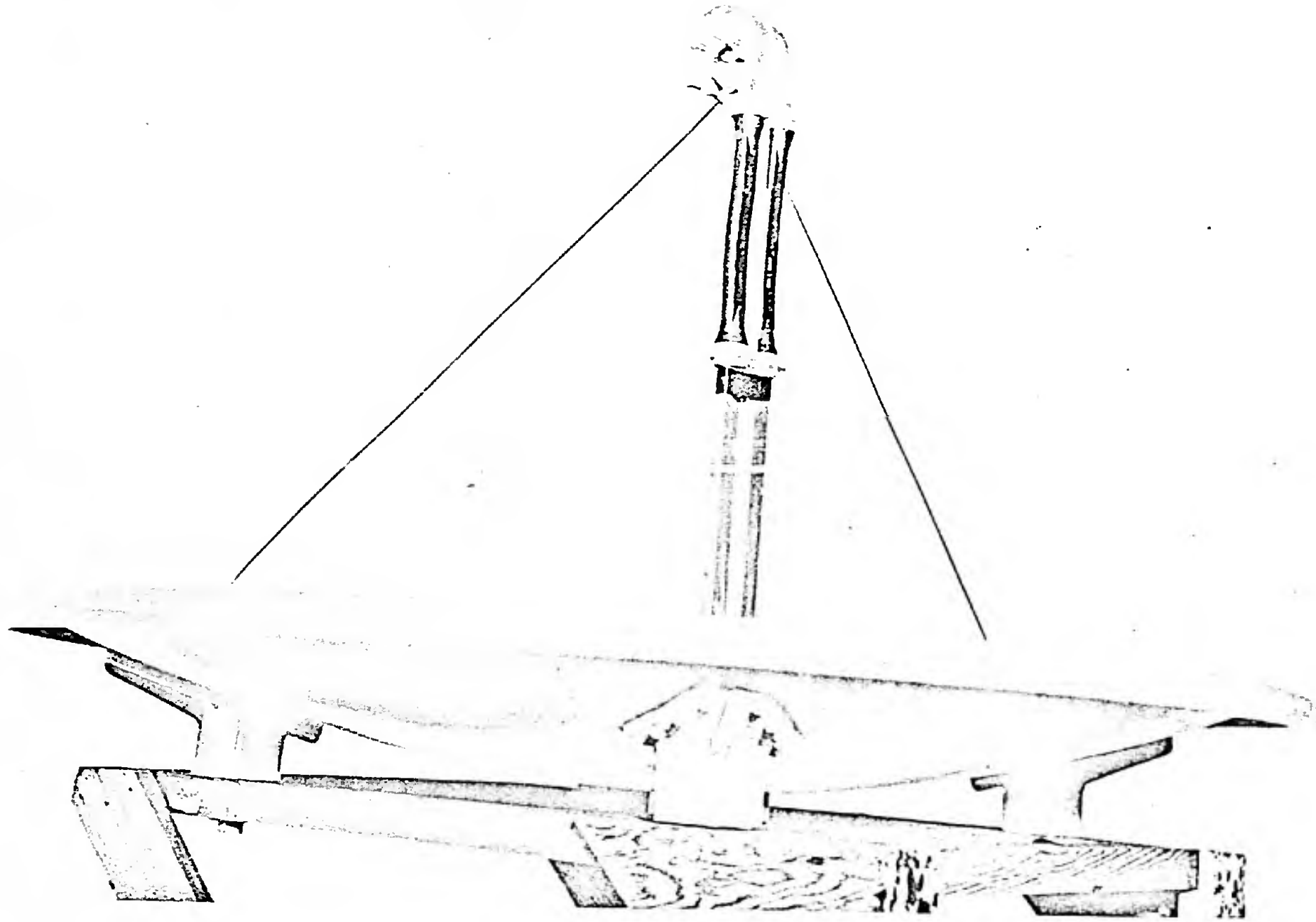

Figure 2

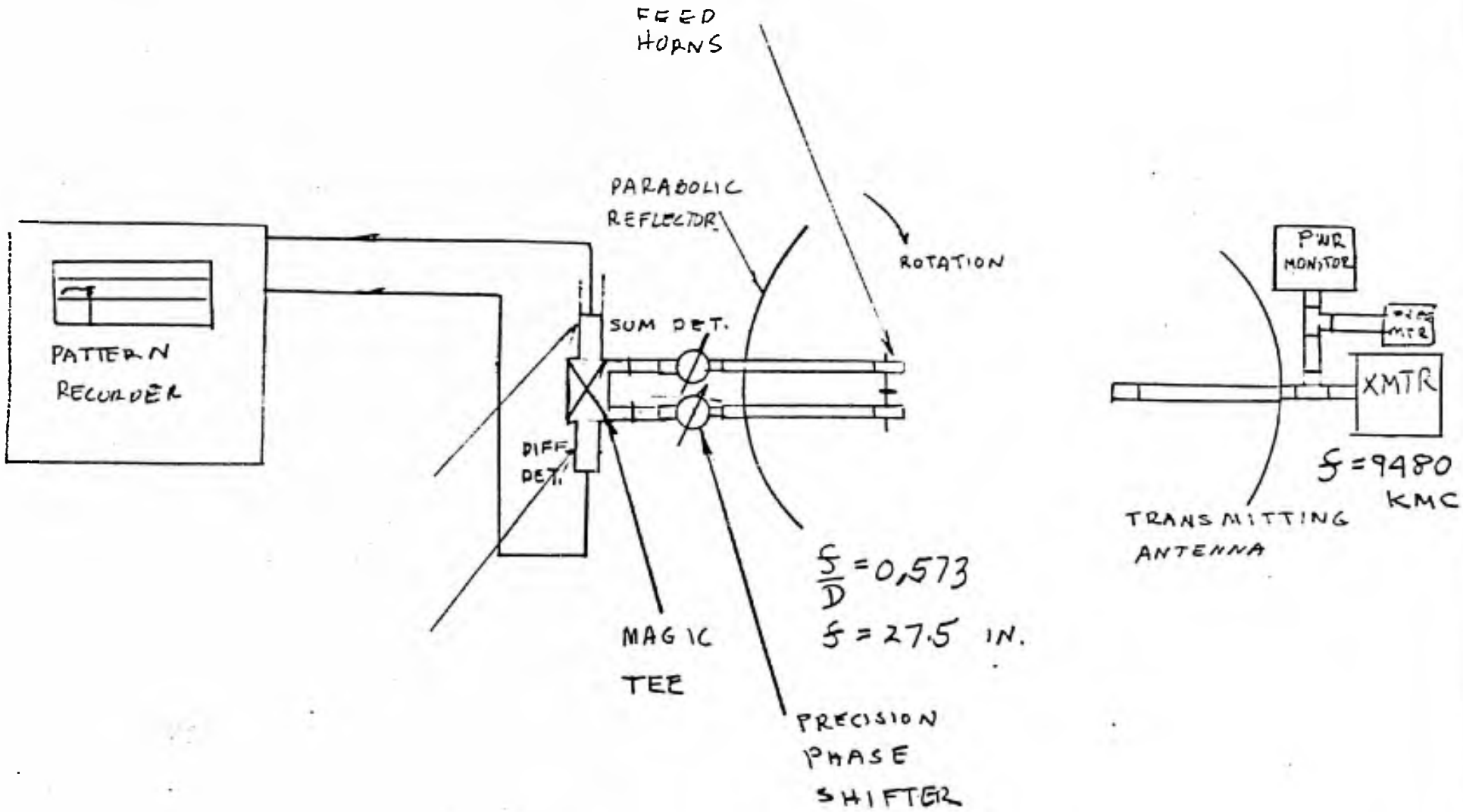

FIGURE 3

EXPERIMENTAL MONOPULSE MODEL

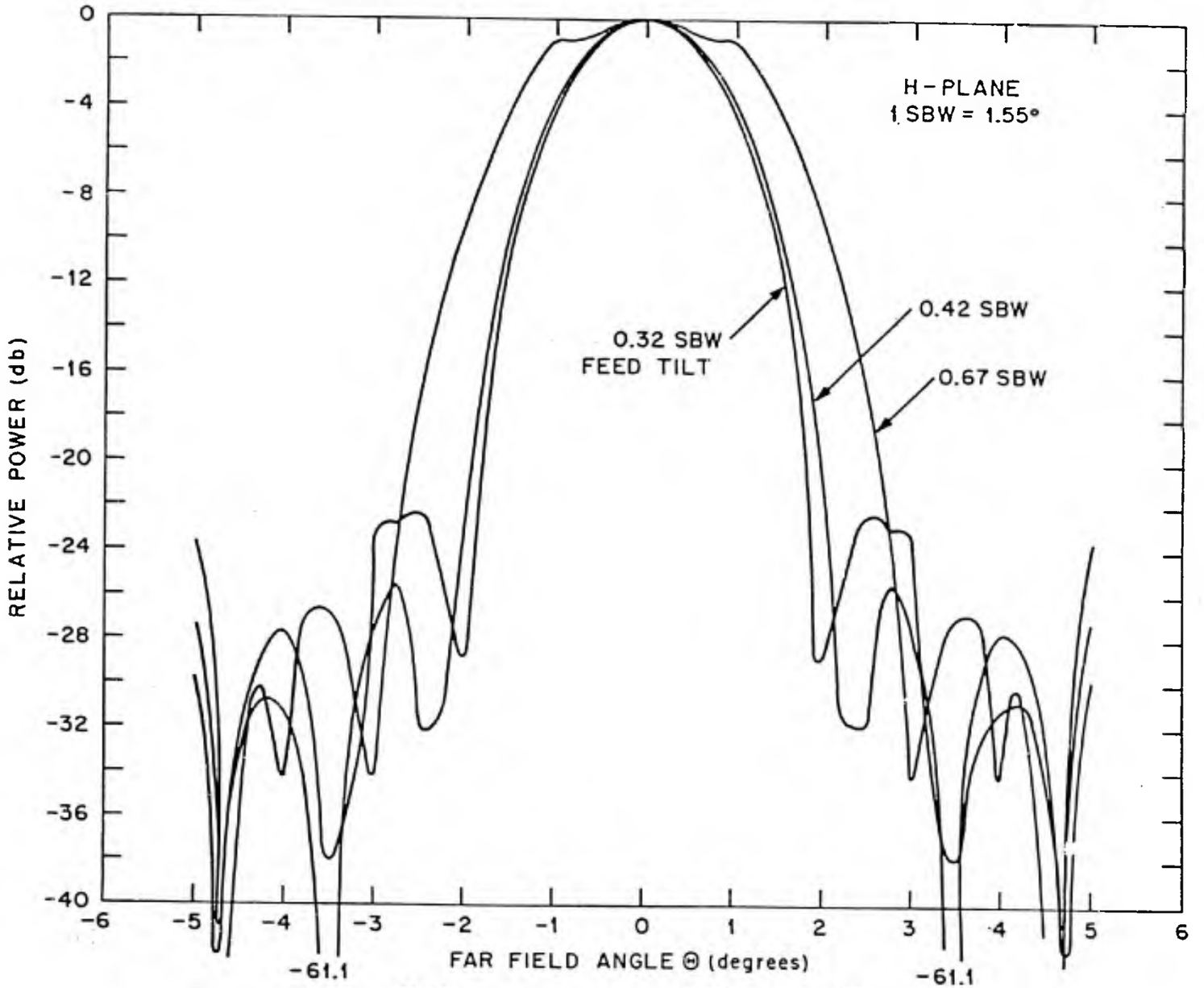

THEORETICAL SUM PATTERNS AS FUNCTION OF FEED TILT
NORMALIZED (CURRENT DIST. METHOD)

GRAPH 1

B-10778-5

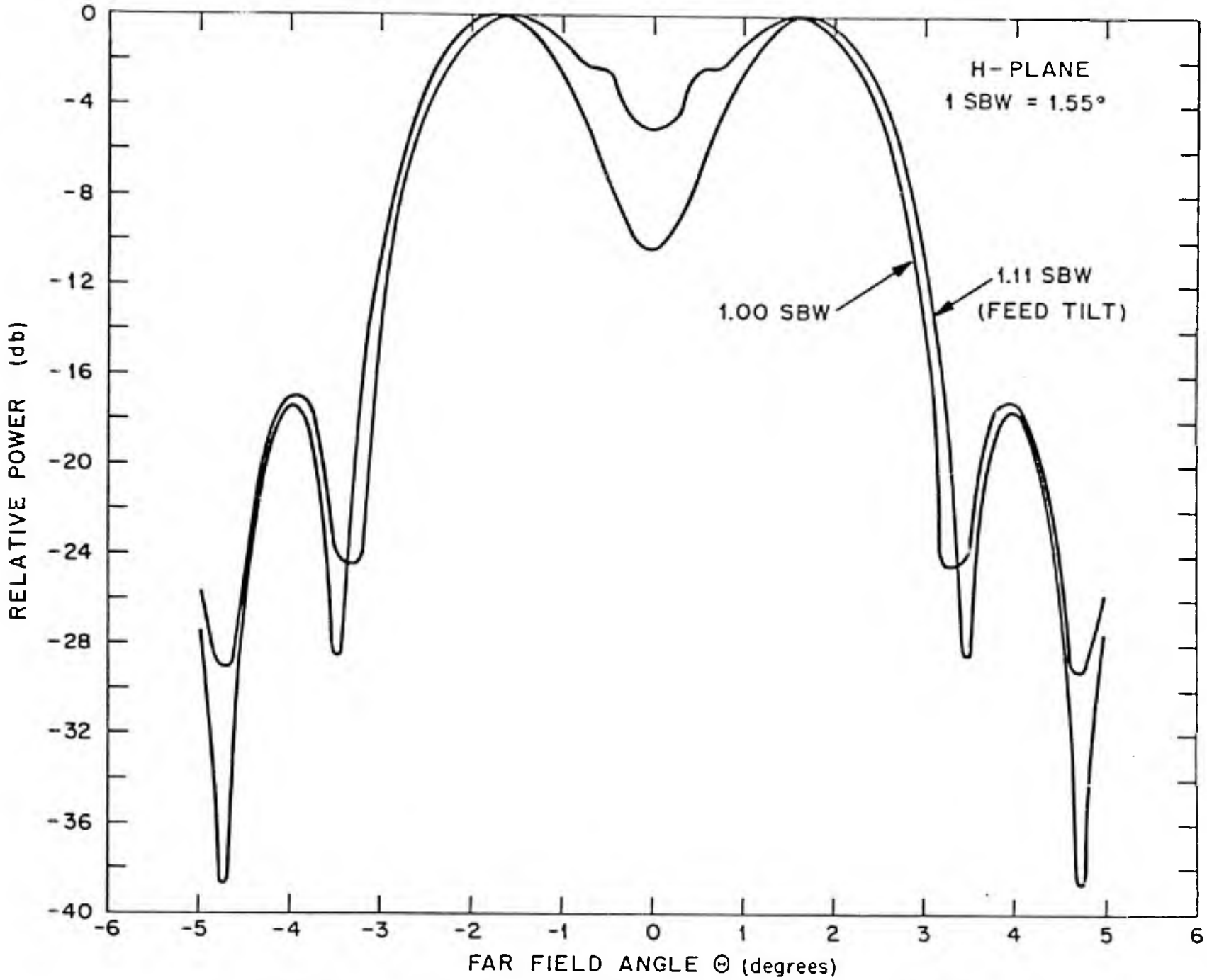

THEORETICAL SUM PATTERNS AS FUNCTION OF FEED TILT
NORMALIZED (CURRENT DIST. METHOD)

GRAPH 2

B-10778-4

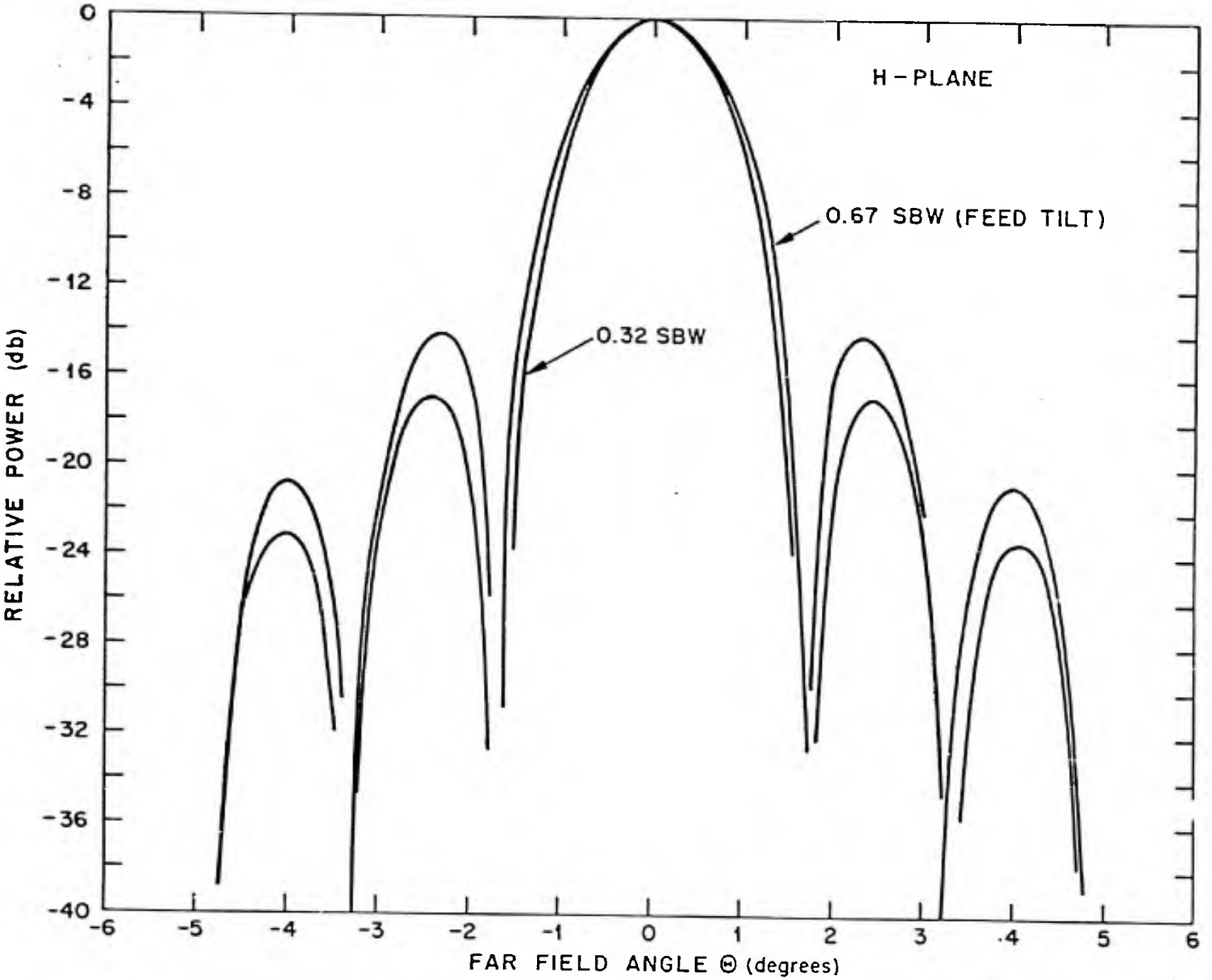

THEORETICAL SUM PATTERNS AS FUNCTION OF FEED TILT
NORMALIZED (SCALAR DIFF. THEORY)

GRAPH 3

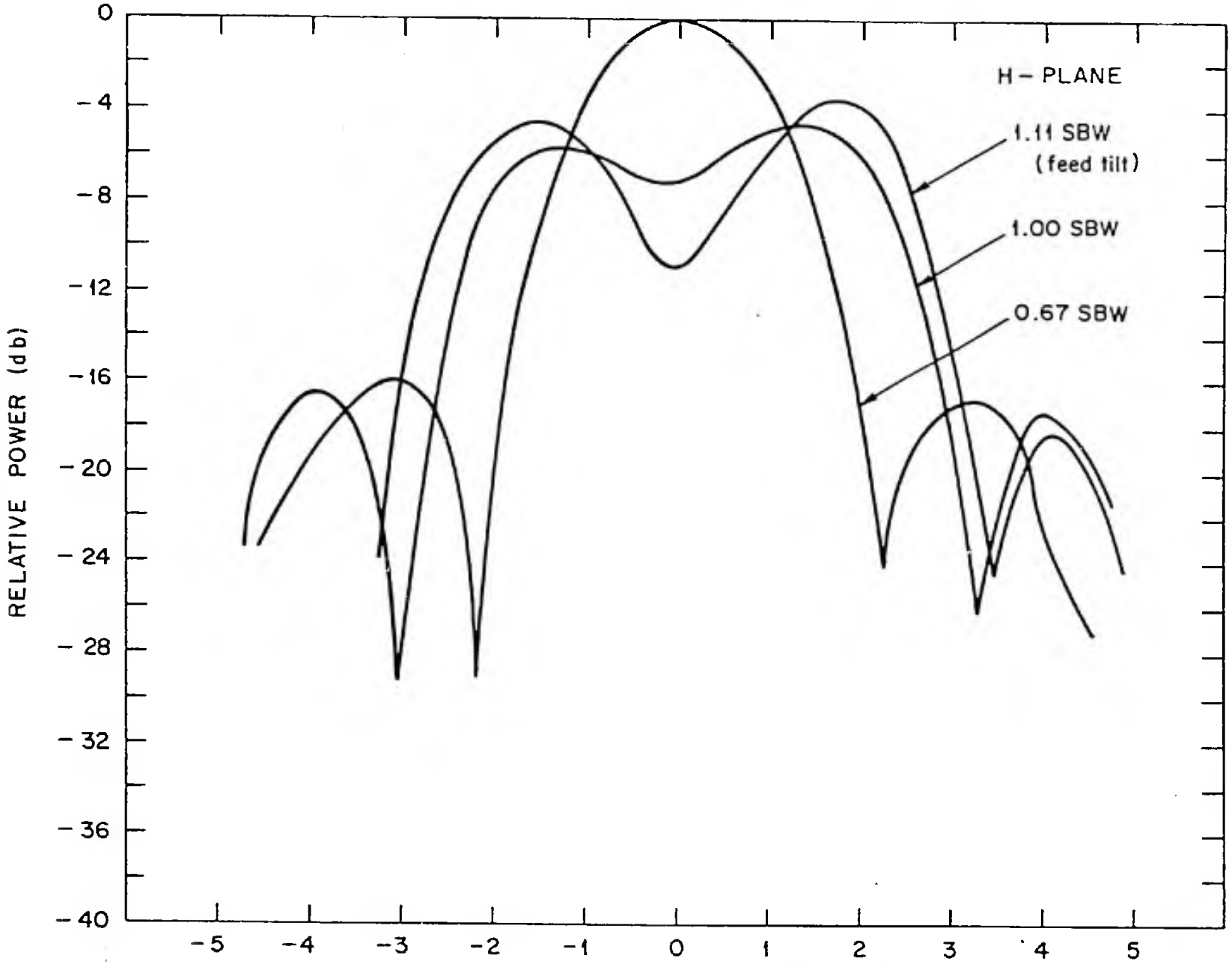

EXPERIMENTAL SUM PATTERNS

GRAPH 4

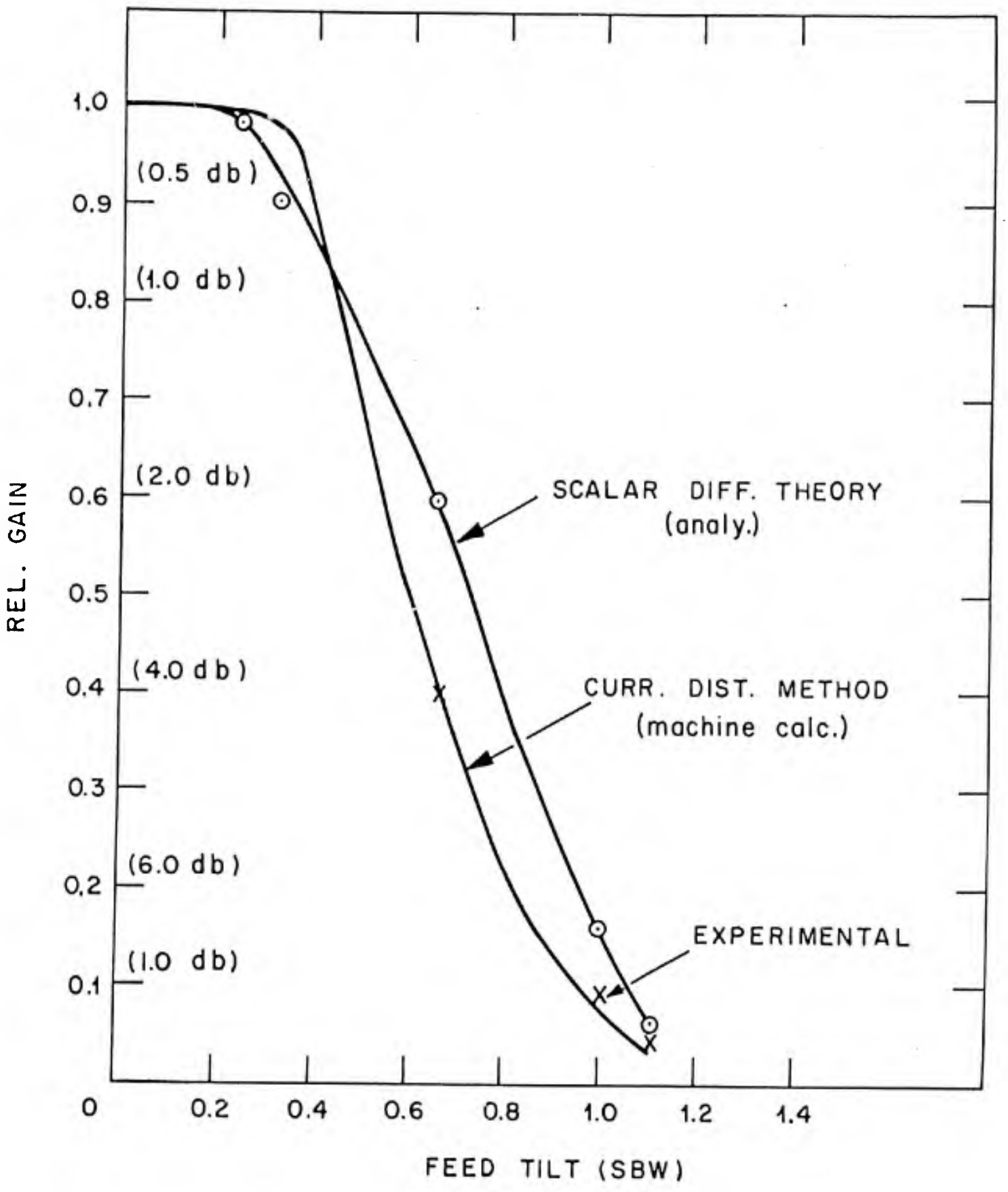

RELATIVE SUM PATTERN GAIN VS. FEED TILT

GRAPH 5

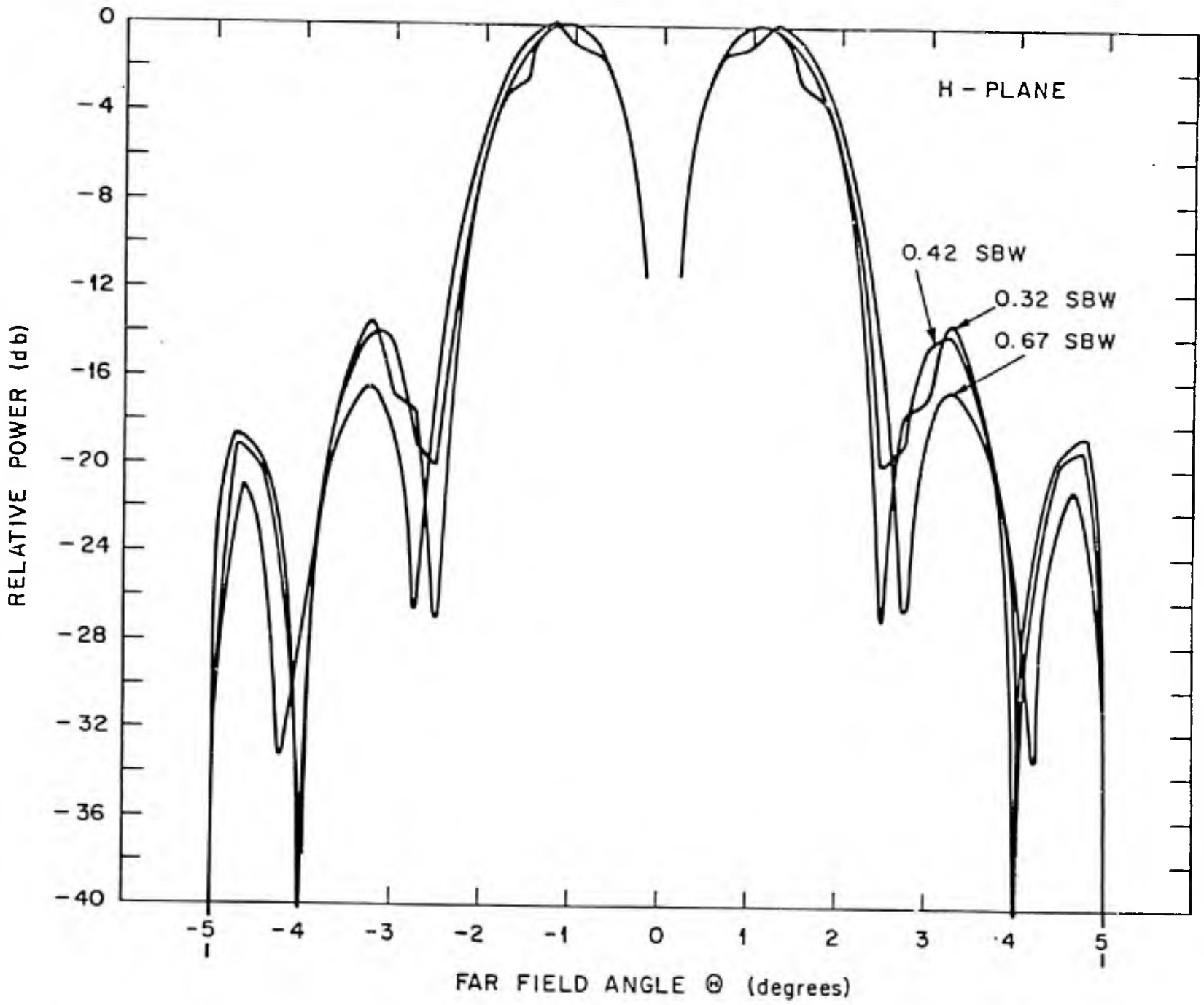

THEORETICAL DIFFERENCE PATTERNS AS FUNCTION OF FEED TILT NORMALIZED (CURRENT DIST. METH.)

GRAPH 6

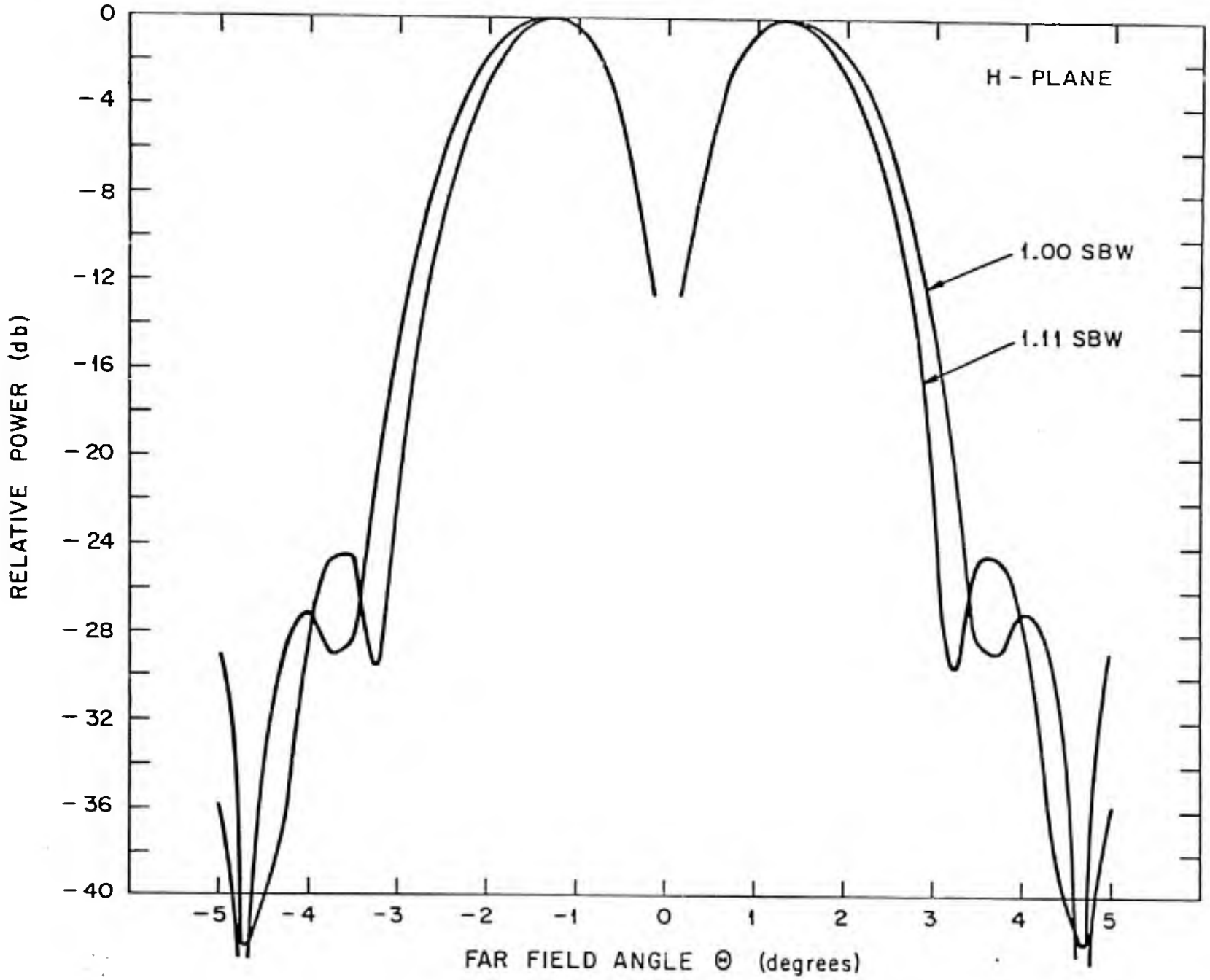

THEORETICAL DIFFERENCE PATTERNS AS FUNCTION OF FEED TILT NORMALIZED (CURRENT DIST. METH.)

GRAPH 7

8-10778-2

BLANK PAGE

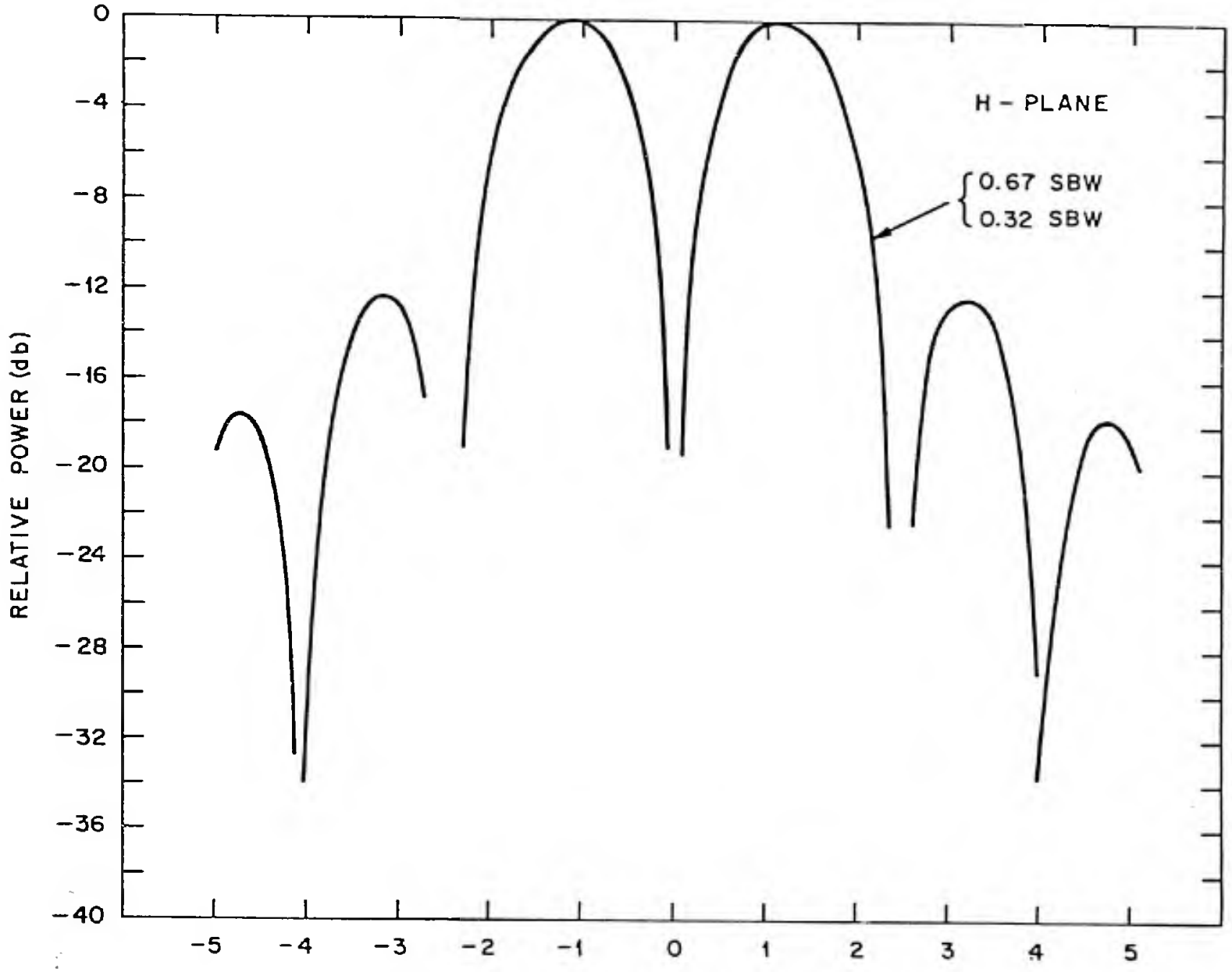

THEORETICAL DIFFERENCE PATTERN (SCALER DIFF. THEORY)

GRAPH 8

BLANK PAGE

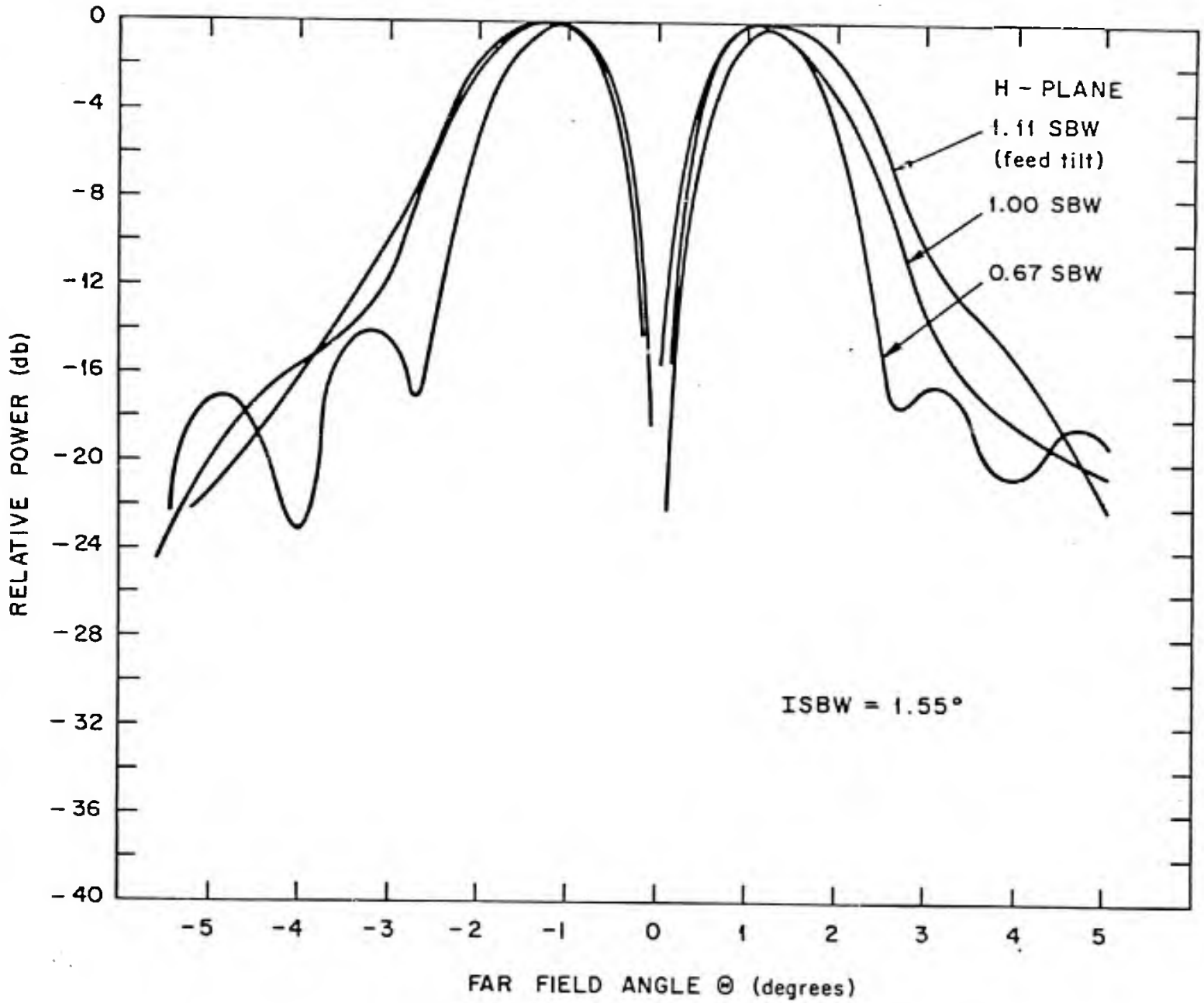

EXPERIMENTAL DIFFERENCE PATTERNS

GRAPH 9

BLANK PAGE

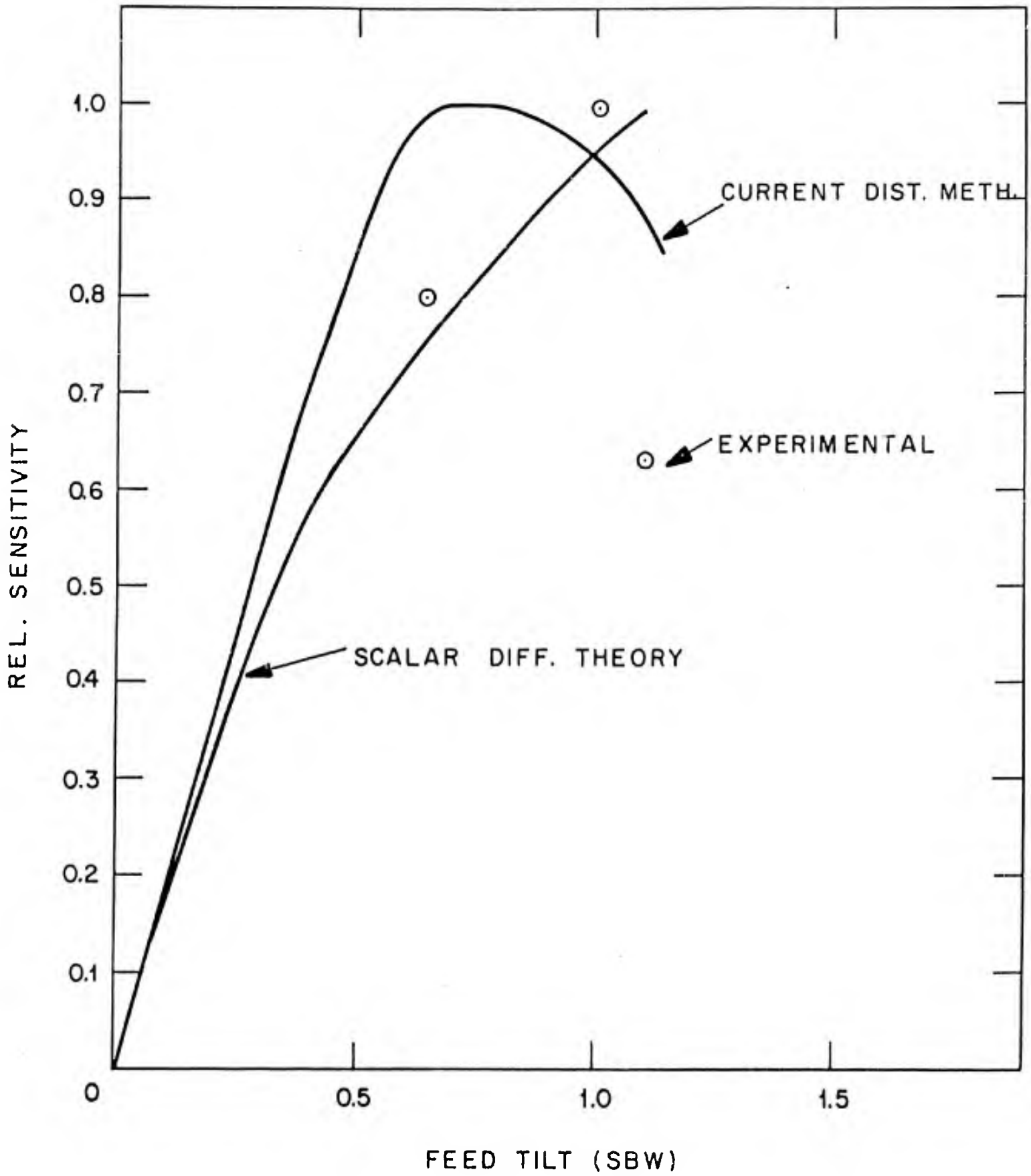

RELATIVE BORESIGHT SENSITIVITY vs. FEED TILT
(diff. pattern) H-PLANE

GRAPH 10

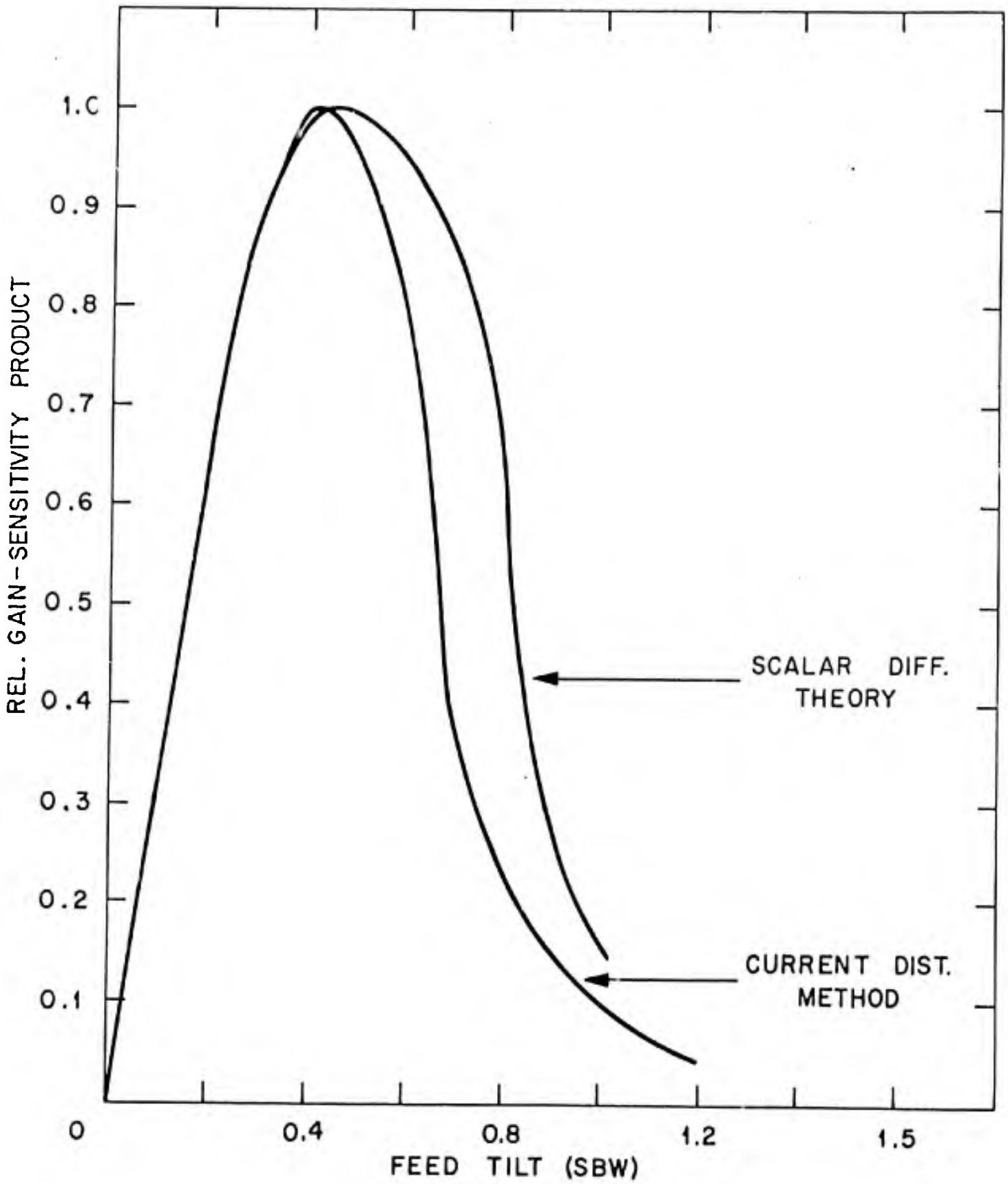

GAIN - SENSITIVITY PRODUCT AS A FUNCTION OF FEED TILT

GRAPH 11